

Numerical Simulations Based on the Mie Scattering Theory for the Time-Harmonic Maxwell's Equations

Alexander Heinlein^[0000-0003-1578-8104],
Sebastian Kinnewig^[0000-0002-0923-7413],
Thomas Wick^[0000-0002-1102-6332]

1 Introduction

We propose a configuration to validate solver methods for Maxwell's equations that involves computing the near-field around a nanoparticle. Besides numerical computations, a reference solution itself can be computed using Mie's scattering [18] theory.

Mie scattering theory is a well-established method for calculating the scattering of electromagnetic waves by spherical particles. It provides an analytical solution to the scattering problem in the form of an infinite series expansion and can be easily computed, making it an ideal reference for validating numerical methods. Here we use the software Scattnlay [16, 15] to compute the reference solution based on Mie's scattering theory. As an application example, we compare the resulting near-field with numerical solutions obtained by the finite element method (FEM). Therein, the Time-Harmonic Maxwell's Equations (THM) must be computed, for which we need Nédélec finite elements [20, 21].

To compute the FEM-based solution, we use the finite-element library deal . II [1, 3] and we refer specifically to our implementation efforts over the last three years for sustainable codes in deal . II that work on globally refined as well as locally refined meshes. Those algorithmic advancements are described and outlined in [13, 14]. The resulting linear system is solved with FROSch (Fast and Robust Overlapping

Alexander Heinlein
TU Delft, DIAM, Faculty of EEMCS Numerical Analysis, Mekelweg 4, 2628 Delft, The Netherlands, e-mail: a.heinlein@tudelft.nl

Sebastian Kinnewig
Leibniz University Hannover, Institute for Applied Mathematics, Welfengarten 1, 30167 Hannover, Germany, e-mail: kinnewig@ifam.uni-hannover.de

Thomas Wick
Leibniz University Hannover, Institute for Applied Mathematics, Welfengarten 1, 30167 Hannover, Germany, e-mail: thomas.wick@ifam.uni-hannover.de

Schwarz) [11, 12] a parallel domain decomposition preconditioning package, which is part of the Trilinos software library [17], that is accessed via the deal.II-FROSch interface [10, 13].

2 Time-Harmonic Maxwell's Equations

In the following, we introduce the weak form of the Time-Harmonic Maxwell's Equations (THM) used in the FEM. We consider $\Omega \subset \mathbb{R}^3$ to be a bounded Lipschitz domain with a sufficiently smooth boundary. The boundary $\Gamma = \Gamma^\infty \cup \Gamma^{\text{inc}}$ is split in the absorbing boundary conditions Γ^∞ , and the incident boundary conditions Γ^{inc} . One simple choice for the absorbing boundary conditions is Robin-type boundary conditions of the form:

$$\mu^{-1} (\mathbf{n} \times (\text{curl}(\mathbf{u}))) - i\sqrt{\varepsilon}\omega (\mathbf{n} \times (\mathbf{u} \times \mathbf{n})) = 0. \quad (1)$$

These correspond to the first-order approximation of the Sommerfeld radiation conditions.

The THM is given by, find $\mathbf{u} \in \mathbf{H}_{\text{curl}}(\Omega)$ such that, for all $\boldsymbol{\varphi} \in \mathbf{H}_{\text{curl}}(\Omega)$ it holds:

$$\begin{aligned} & \int_{\Omega} \left(\mu^{-1} \text{curl}(\mathbf{u}) \cdot \text{curl}(\boldsymbol{\varphi}) - \varepsilon\omega^2 \mathbf{u} \cdot \boldsymbol{\varphi} \right) dx \\ & + i\sqrt{\varepsilon}\omega \int_{\Gamma} (\mathbf{n} \times (\mathbf{u} \times \mathbf{n})) \cdot (\mathbf{n} \times (\boldsymbol{\varphi} \times \mathbf{n})) ds, \\ & = \int_{\Gamma^{\text{inc}}} (\mathbf{n} \times (\mathbf{u}^{\text{inc}} \times \mathbf{n})) \cdot (\mathbf{n} \times (\boldsymbol{\varphi} \times \mathbf{n})) ds. \end{aligned} \quad (2)$$

Here the incident boundary condition is described by \mathbf{u}^{inc} with $\mathbf{n} \times \mathbf{u}^{\text{inc}} \in L^2(\Gamma^{\text{inc}}, \mathbb{C}^d)$. Moreover, i is the imaginary number, $\varepsilon \in \mathbb{R}^+$ is the relative permittivity, $\mu \in \mathbb{R}^+$ is the relative magnetic permeability, $\omega = \frac{2\pi}{\lambda}$ is the angular wavenumber, and $\lambda \in \mathbb{R}^+$ is the wavelength. For a detailed derivation of the THM, we refer to [19].

3 Optimized Schwarz Preconditioners

Employing the Finite Element Method (FEM) to discretize boundary value problems on some computational domain Ω results at some point in sparse linear equation systems of the form

$$Ax = b. \quad (3)$$

For future reference, we use h to represent the mesh parameter, and the finite element space is denoted as $V := V^h(\Omega)$.

Solving wave-type problems with FEM is challenging and requires suitable solver methods [7]. One prominent approach is based on domain decomposition methods, especially on optimized additive Schwarz (OAS) and optimized restricted additive Schwarz (ORAS) preconditioners [22]. Especially for wave-type problems, standard additive Schwarz preconditioners often lead to suboptimal convergence rates compared to optimized Schwarz preconditioners.

Let us consider the THM equations

$$\text{curl}(\text{curl}(\mathbf{u})) - \varepsilon\omega^2\mathbf{u} = \mathbf{f} \quad \text{in } \Omega,$$

where \mathbf{f} is a source term and we assume suitable boundary conditions on $\partial\Omega$. We decompose Ω into N non-overlapping subdomains $\Omega_1, \dots, \Omega_N$. In practice, this decomposition may, for instance, be obtained via a geometrical approach or via partitioning the dual graph of the triangulation using a graph partitioning tool, such as p4est [6]. We denote the size of the overlap by $\delta = kh$ and define the local finite element spaces V_i on the local overlapping subdomains. Due to our construction, it follows that $V_i \subset V$, and we can define restriction operators $R_i : V \rightarrow V_i$ and corresponding prolongation operators $P_i : V_i \rightarrow V$, for all $1 \leq i \leq N$. Both can be represented as sparse binary matrices, and $P_i = R_i^\top$ is the transposed operator of R_i . In particular, the OAS preconditioner reads

$$M_{\text{OAS}}^{-1} = \sum_{i=1}^N P_i B_i^{-1} R_i, \tag{4}$$

and the ORAS preconditioner reads

$$M_{\text{ORAS}}^{-1} = \sum_{i=1}^N P_i D_i B_i^{-1} R_i, \tag{5}$$

where D_i is a binary, diagonal scaling matrix, and in the most simple case, the matrix B_i is the discretization of the differential operator $\text{curl}(\text{curl}(\mathbf{u})) - \varepsilon\omega^2\mathbf{u}$ using the local finite element space V_i and with Robin boundary operator $\left(\frac{\partial}{\partial n} + \alpha\right)$, $\alpha \in \mathbb{R}$, on the nodes of $\partial\Omega'_i \setminus \partial\Omega$. α is the Robin parameter, which can be tuned and gives the method its name. In practice, the optimization can be done either theoretically [8] or computationally via numerical calibration. In a Krylov iteration, the application of B_i^{-1} typically corresponds to solving a system of the form

$$B_i y_i = R_i (b - Ax^{(k)}),$$

for y_i . The right-hand side is a restriction of the residual to Ω'_i , and $x^{(k)}$ is the iterate in the k th iteration. In particular, the restriction R_i is chosen such that $R_i (b - Ax^{(k)}) = 0$ for the nodes on $\partial\Omega'_i \setminus \partial\Omega$. As a result, we enforce the Robin boundary condition

$$\left(\frac{\partial}{\partial n} + \alpha\right) = 0 \tag{6}$$

on those nodes.

Other boundary conditions employing a perfectly matched layer (PML) [5] or other types of absorbing boundary conditions [9], are more complex and depend on more than one parameter, but may yield even better convergence than Robin boundary conditions. In all optimized Schwarz methods, the matrix B_i cannot be obtained algebraically. Instead, the local system matrix has to be assembled separately to construct the preconditioner, making this method rather complicated to implement. Therefore, it is not feasible to implement such a method from scratch; rather, we use `deal.II-FROSch` interface introduced in [10, 13], to solve the scattering problem.

4 Numerical Simulations

For the configuration, we assume a silver particle surrounded by air. The computational domain is given by $\Omega = [-200 \text{ nm}, 200 \text{ nm}]^3$, and the silver particle is located at the center of the computational domain and given by $\Omega_{\text{particle}} := \{(\mathbf{x} \in \Omega \mid \|\mathbf{x}\| < 100 \text{ nm})\}$. Note that we assume the origin of the coordinate system to be at the center of the silver particle. The nanoparticle has a refractive index of $r_{\text{Ag}} = 0.0 + 4.0i$, and the surrounding air has a refractive index of $n_{\text{air}} = 1.0$. As the incident field, we consider a planar wave with a wavelength of $\lambda = 250 \text{ nm}$ and linear polarization in the y -direction on $\Gamma_{\text{inc}} = \{-200\} \times [-200, 200] \times [-200, 200] \text{ nm}$ and absorbing boundary conditions on all other boundaries. The geometry is shown in Fig. 1 (left). In `deal.II` we use a `SphericalManifold` to create the particle.

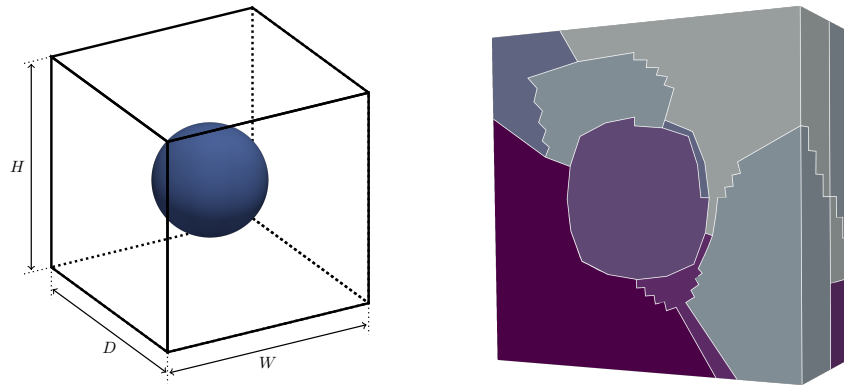


Fig. 1 Left: A silver particle with a radius of 100 nm surrounded by air, of which we compute the near-field scattering when it is hit by a planar electromagnetic wave. **Right:** Visualization of the considered domain decompositions. An automatically generated domain decomposition is used with the ORAS preconditioner.

Mie theory, developed by the German physicist Gustav Mie in 1908, is a fundamental analytical method for calculating the scattering of plane electromagnetic

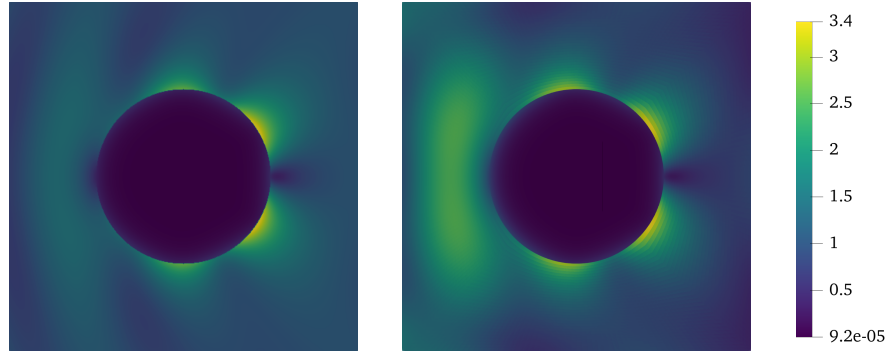


Fig. 2 The x - y cross-section of the intensity of an electric field scattered from a silver ball in a vacuum, computed with the optimized Schwarz method on an adaptively refined grid. **Left:** The resulting electric field, computed via Scattnlay, based on Mie's theory. **Right:** The solution computed with the ORAS preconditioner.

waves by spherical particles [18]. It is widely used in various fields, including atmospheric science, biomedical optics, and nanotechnology, as detailed in [4, Chapter 4]. The key components of Mie's theory include calculating scattering coefficients, scattering amplitudes, and cross sections, which describe the particle's efficiency in scattering, absorbing, and extinguishing the incident light. The resulting electric field, computed via Scattnlay, is shown in Fig. 2 (left).

The following results were computed using the `deal.II-FROSch` [10, 13], which utilizes the ORAS preconditioner as introduced in Section 3. The resulting near-field around the nanoparticle is shown in Fig. 2. The electric field intensity is similar to the solution computed with the ORAS method, as shown in Fig. 3. The difference between the result computed with the optimized Schwarz method and the solution computed with Scattnlay is due to the absorbing boundary conditions. As discussed in Section 2, the Robin-type boundary conditions correspond to a first-order approximation of the absorbing boundary conditions.

4.1 Physics Results

As validation of the method, one can compute a reference based on Mie's theory, e.g., by using Scattnlay [16]. Moreover, we provide three point values and the L^2 -norm of the solution inside of the particle as a reference. For the point evaluation, we consider the intensity of the electric field in front of the silver ball at $P_{(-150,0,0)}$, and behind the silver ball $P_{(150,0,0)}$, and the L^2 -norm of the electric field inside of the silver ball $\|u_{\text{ORAS}}\|_{L^2(\Omega_{\text{particle}})}$. These values are provided in Table 1.

In comparison between the solution computed with Scattnlay, shown in Fig. 2 (left), and the solution computed with ORAS, shown in Fig. 2 (right), the main features of the solution match. Nevertheless, there are some differences between

Table 1 Overview of the reference values on different refinement levels.

DoFs	$ P_{(-150,0,0)} $	$ P_{(150,0,0)} $	$\ u_{\text{ORAS}}\ _{L^2(\Omega_{\text{particle}})}$
175 264	0.69369	0.15696	0.0070596
1 388 864	0.70086	0.16449	0.0071176
11 059 840	0.70257	0.16678	0.0070593

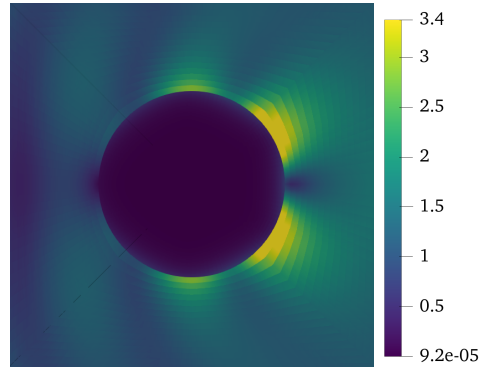


Fig. 3 The x-y cross-section of the intensity of an electric field scattered from a silver ball in a vacuum. The solution was computed on the domain $[-400 \text{ nm}, 400 \text{ nm}]^3$. However, we restrict our focus on the same domain as the other solutions displayed in Figure 2 for better comparison. The left part of the ball is much closer to Scattnlay, while the right part slightly differs due to the coarser overall resolution due to the domain increase.

these solutions, which can be quantified by considering the L^2 difference:

$$\|u_{\text{ORAS}} - u_{\text{Mie}}\|_{L^2(\Omega)} = 0.083,$$

where u_{ORAS} is the numerical solution and u_{Mie} Mie's analytical solution, obtained from the Mie theory calculator web application¹. This difference arises from the discretization error and the use of Robin-type boundary conditions as absorbing boundary conditions. To validate the influence of the Robin-type boundary conditions, we compute the near-field in the domain $[-400 \text{ nm}, 400 \text{ nm}]^3$. The result is shown in Fig. 3. The result shows a better agreement with the solution from Scattnlay.

4.2 Solver Analysis

To evaluate the performance of the ORAS preconditioner, we investigate the number of GMRES iterations and computing times in a weak scalability study. In particular, we consider one subdomain per MPI rank and vary the number of subdomains

¹ <https://github.com/ovidiopr/scattnlay>

Table 2 Overview of the wall times and the number of GMRES iterations required to solve the near-field problem around the nanoparticle using the ORAS preconditioner, depending on the number of ranks, which corresponds to the number of subdomains.

# ranks	DoFs	overlap width 5 %		overlap width 10 %		overlap width 20 %	
		n^{GMRES}	t^{walltime}	n^{GMRES}	t^{walltime}	n^{GMRES}	t^{walltime}
2	175 264	14	1.6 min	11	1.7 min	9	2.0 min
16	1 388 864	> 1000	–	30	2.4 min	23	3.6 min
128	11 059 840	> 1000	–	> 1000	–	181	21.0 min

(resp. MPI ranks) while keeping the number of DoFs per non-overlapping subdomain fixed. In three dimensions, this is achieved by a single global refinement and an eightfold increase in the number of subdomains. Furthermore, to investigate the influence the impact of the overlap, we vary the number of layers of overlap k . The stopping tolerance for the absolute residual of GMRES is chosen as 10^{-12} .

The presented results were computed on a server with a $2 \times$ AMD EPYC 7H12 64-Core processor and 1024 GB of RAM. As a subdomain solver for the domain decomposition method, the direct solver MUMPS [2], called in serial, was used. As an iterative solver, the default GMRES solver of deal.II was used, where the size of the Arnoldi basis is set to 30; preconditioning is done from the left, and re-orthogonalization is only done if necessary.

The computation of the near-field around a nanoparticle is a challenging application. As described above, we have seen the influence of the absorbing boundary conditions. Next, we examine the number of GMRES iterations required when using the ORAS preconditioner. The results are reported in Table 2. Here, the overlap width is chosen relative to the subdomain size; hence, we report H/h . On the finest level with around 11 million DoFs, an overlap of $\delta \approx 20\%$ was required for GMRES to converge under 1000 steps. In this case, the assembly of the global system matrix took 274 seconds, the assembly of the local matrices took around 126 seconds, the computation of the preconditioner took around 932 seconds, and solving the global linear system took around 964 seconds. Note that, due to an suboptimal choice of the Robin parameter in the transmission boundary conditions of the overlapping subdomain problems, we require an overlap of 20% for GMRES to converge within 1000 iterations. We made this choice because, in small-wavelength test cases, the parameter had only a minor influence. However, in the present work, where the wavelength is large compared to the computational domain, the Robin parameter is expected to have a stronger impact on the convergence rate. Therefore, optimizing the Robin parameter could improve solver performance. This is left for future work.

References

1. Africa, P.C., Arndt, D., Bangerth, W., Blais, B., Fehling, M., Gassmüller, R., Heister, T., Heltai, L., Kinnewig, S., Kronbichler, M., et al.: The deal.ii library, version 9.6. J. Numer. Math. **32**(4)

- (2024)
2. Amestoy, P.R., Buttari, A., L'Excellent, J.Y., Mary, T.: Performance and scalability of the block low-rank multifrontal factorization on multicore architectures. *ACM Trans. Math. Softw.* **45**(1), 2:1–2:26 (2019)
 3. Arndt, D., Bangerth, W., Davydov, D., Heister, T., Heltai, L., Kronbichler, M., Maier, M., Pelteret, J.P., Turcksin, B., Wells, D.: The deal.II finite element library: design, features, and insights. *Comput. Math. Appl.* (2020)
 4. Bohren, C.F., Huffman, D.R.: Absorption and scattering of light by small particles, 1 edn. Wiley (1998)
 5. Bootland, N., Borzooei, S., Dolean, V., Tournier, P.H.: Numerical assessment of PML transmission conditions in a domain decomposition method for the Helmholtz equation. In: *Domain Decomposition Methods in Science and Engineering XXVII*, pp. 445–453. Springer (2024)
 6. Burstedde, C., Wilcox, L.C., Ghattas, O.: p4est: scalable algorithms for parallel adaptive mesh refinement on forests of octrees. *SIAM J. Sci. Comput.* **33**(3), 1103–1133 (2011)
 7. Ernst, O.G., Gander, M.J.: Why it is difficult to solve Helmholtz problems with classical iterative methods. In: *Numerical analysis of multiscale problems, Lect. Notes Comput. Sci. Eng.*, vol. 83, pp. 325–363. Springer (2012)
 8. Gander, M.J.: Optimized Schwarz methods. *SIAM J. Numer. Anal.* **44**(2), 699–731 (2006)
 9. Gander, M.J., Zhang, H.: Optimized Schwarz methods with overlap for the Helmholtz equation. *SIAM J. Sci. Comput.* **38**(5), A3195–A3219 (2016)
 10. Heinlein, A., Kinnewig, S., Wick, T.: Coupling deal.ii and FROSch: a sustainable and accessible (o)ras preconditioner. *ACM Trans. Math. Softw.* (2025)
 11. Heinlein, A., Klawonn, A., Rajamanickam, S., Rheinbach, O.: FROSch: a fast and robust overlapping Schwarz domain decomposition preconditioner based on Xpetra in Trilinos. In: *Domain Decomposition Methods in Science and Engineering XXV, Lect. Notes Comput. Sci. Eng.*, vol. 138, pp. 176–184. Springer (2020)
 12. Heinlein, A., Klawonn, A., Rheinbach, O.: A parallel implementation of a two-level overlapping Schwarz method with energy-minimizing coarse space based on Trilinos. *SIAM J. Sci. Comput.* **38**(6), C713–C747 (2016)
 13. Kinnewig, S.: Domain decomposition solvers for electromagnetic and multiphysics problems. Ph.D. thesis, Leibniz University Hannover (2025)
 14. Kinnewig, S., Wick, T., Beuchler, S.: Algorithmic realization of the solution to the sign conflict problem for hanging nodes on hp-hexahedral Nédélec elements. *ACM Trans. Math. Softw.* (2025)
 15. Ladutenko, K., Pal, U., Rivera, A., Peña-Rodríguez, O.: Mie calculation of electromagnetic near-field for a multilayered sphere. *Comput. Phys. Commun.* **214**, 225–230 (2017)
 16. Ladutenko, K., Peña Rodríguez, O., Müller, P., Badger, T.G.: ovidiopr/scattnlly: the second stable release (2017)
 17. Mayr, M., Heinlein, A., Glusa, C., Rajamanickam, S., Arnst, M., Bartlett, R., Berger-Vergiat, L., Boman, E., Devine, K., Harper, G., Heroux, M., Hoemmen, M., Hu, J., Kelley, B., Kim, K., Kouri, D.P., Kuberry, P., Liegeois, K., Ober, C.C., Pawlowski, R., Pearson, C., Perego, M., Phipps, E., Ridzal, D., Roberts, N.V., Siefert, C., Thornquist, H., Tomasetti, R., Trott, C.R., Tuminaro, R.S., Willenbring, J.M., Wolf, M.M., Yamazaki, I.: Trilinos: enabling scientific computing across diverse hardware architectures at scale (2025)
 18. Mie, G.: Beiträge zur Optik trüber Medien, speziell kolloidaler Metallösungen. *Ann. Phys.* **330**(3), 377–445 (1908)
 19. Monk, P.: Finite element methods for Maxwell's equations. *Numerical Mathematics and Scientific Computation*. Oxford University Press, Oxford; New York (2003)
 20. Nédélec, J.C.: Mixed finite elements in \mathbb{R}^3 . *Numer. Math.* **35**(3), 315–341 (1980)
 21. Nédélec, J.C.: A new family of mixed finite elements in \mathbb{R}^3 . *Numer. Math.* **50**, 57–81 (1986)
 22. St-Cyr, A., Gander, M.J., Thomas, S.J.: Optimized multiplicative, additive, and restricted additive Schwarz preconditioning. *SIAM J. Sci. Comput.* **29**(6), 2402–2425 (2007)